Polyhedron 85 (2015) 196–207

Contents lists available at ScienceDirect

Polyhedron

journal homepage: www.elsevier.com/locate/poly

Binuclear dioxomolybdenum(VI) complexes of some tridentate ONS donor ligand containing $[MoO_2]^{2+}$ as the acceptor center: Synthesis, crystal structure, supramolecular architectures via hydrogen bonds, π-π stacking and DFT calculations

Nikhil Ranjan Pramanik [a,*], Manashi Chakraborty [b], Debanjana Biswal [c], Sudhanshu Sekhar Mandal [c,*], Saktiprosad Ghosh [c], Syamal Chakrabarti [c], William S. Sheldrick [d], Michael G.B. Drew [e], Tapan Kumar Mondal [f], Deblina Sarkar [f]

[a] Department of Chemistry, Bidhannagar College, EB-2, Salt Lake, Kolkata 700064, India
[b] Department of Chemistry, NITMAS, Jhinga, P.O. Amira, Diamond Harbour Road, District 24 Pgs. (S), West Bengal 743368, India
[c] Department of Chemistry, University College of Science, 92, Acharya Prafulla Chandra Road, Kolkata 700009, India
[d] Lehrstuhl fur Analytische Chemie, Ruhr-Universitat Bochum, D-44780 Bochum, Germany
[e] Department of Chemistry, The University of Reading, Whiteknights, Reading RG66AD, UK
[f] Department of Chemistry (Inorganic Section), Jadavpur University, Kolkata 700032, India

ARTICLE INFO

Article history:
Received 4 June 2014
Accepted 2 August 2014
Available online 12 August 2014

Keywords:
Dioxomolybdenum(VI) complexes
Supramolecular
Hydrogen bond
π-π stacking
DFT calculations

ABSTRACT

A series of linear diimine and diamine-bridged binuclear dioxomolybdenum(VI) complexes having general formula $[(MoO_2L)_2(B\text{-}B)]$ [where, B-B is a bridging linear N,N′-bidentate spacer 4,4′ bipyridine, 1,2 bis (4-pyridyl) ethene and 1,2 bis (4-pyridyl) ethane] with the tridentate binegative Schiff base ligands obtained by the condensation of salicylaldehyde/2-hydroxyacetophenone with S-benzyl/S-methyl dithiocarbazate have been synthesized. Elemental analysis, various spectroscopic (IR, UV–Vis, ^{1}H NMR) measurements and electrochemical studies have been used for characterization of these complexes. The complexes **2**, **2a**, **9** and **10** were structurally characterized by single crystal X-ray crystallography which reveal that in these complexes the overall coordination geometry around the Mo(VI) center can be described as distorted octahedral. Complexes **2**, **2a**, **9** and **10** give rise to interesting supramolecular architectures via hydrogen bonding and π-π stacking interactions. In addition, extensive hydrogen bonding interactions in complex **10** lead to the formation of cavities. DFT calculations on the ligand and complexes **2**, **2a**, **9** and **10** were also carried out.

1. Introduction

The chemistry of Mo(VI) has enticed special attention because of its relevance to several biological [1,2] and industrial [3–5] processes. Dioxomolybdenum complexes exhibit oxo-transfer ability to some selected substrates and mimic the active centers of some oxo-transfer molybdoenzymes [6]. Syntheses of binuclear complexes in which two redox active centers can undergo electrochemical interaction across a conjugated bridging ligand is of interest for the study of mixed-valence complexes and the eventual development of molecular wires [7]. Linear N,N′-bidentate spacers 4,4′ bipyridine (4,4′ bipy), *trans*-1,2 bis (4-pyridyl) ethene and *trans*-1,2 bis (4-pyridyl) ethane are found to be excellent bridging ligands, each of which can connect two separate coordination spheres of two coordinatively unsaturated metal centers. Though many homo and hetero-metallic diimine-bridged complexes of other transition metals are known [8], most of the binuclear/polynuclear complexes of molybdenum are oxo-, sulfido- and halogeno-bridged. A large number of binuclear molybdenum complexes using extended poly pyridyl type bridging ligands have been reported by Ward and coworkers [9], but the Mo-centers in most of these complexes are in very low oxidation (I/II) states, contain no oxomolybdenum center and many of them are not characterized crystallographically. Zubita and coworkers have synthesized and structurally characterized a few molybdenum(VI) oxide organodiamine compounds [10]. Koo et al. [11,12] have prepared and structurally characterized a few binuclear dioxo molybdenum(VI)

* Corresponding authors. Tel.: +91 033 2337 4389; fax: +91 033 2337 4782.
E-mail address: nr_pramanik@yahoo.co.in (N.R. Pramanik).

http://dx.doi.org/10.1016/j.poly.2014.08.010
0277-5387/

complexes with tridentate ONS donor Schiff base bridged by 4,4′-bipyridyl or its derivatives.

The field of supramolecular chemistry is one of the most frontier and emergent areas of research because of its structural elegance and enormous potential applications [13a,b]. The design and construction of suitable ligands with desirable connectivity for the metal center plays the main role in supramolecular designs. The crystal structures of these complexes often exhibit various interesting supramolecular architectures. Extensive hydrogen bonds and π-π stacking interactions play a pivotal role in the self assembly of the binuclear Mo(VI) complexes.

In this work we have synthesized and structurally characterized some linear diimine and diamine-bridged binuclear Mo(VI) complexes of the type [(MoO_2L)$_2$ (B-B)] [where B-B is a bridging linear N,N′-bidentate spacer 4,4′ bipyridine, 1,2 bis (4-pyridyl) ethene and 1,2 bis (4-pyridyl) ethane]. In the complexes, two MoO_2L units are joined together by a bridging N,N′-bidentate spacer to form a binuclear species (where L = H_2L^1, H_2L^2, H_2L^3 and H_2L^4). The crystal structures of complexes **2**, **2a**, **9** and **10** have been determined by single crystal X-ray diffraction methods. The spectroscopic and electrochemical behavior of these complexes have also been described.

2. Experimental

2.1. Materials

Reagent grade solvents were dried and distilled prior to use. All other chemicals used for preparative work were of reagent grade, available commercially and used without further purification.

2.2. Syntheses

2.2.1. Syntheses of the ligands

The Schiff base ligands (H_2L^1, H_2L^2, H_2L^3 and H_2L^4) were prepared by condensing S-benzyl and S-methyl dithiocarbazates with salicylaldehyde and 2-hydroxyacetophenone in ethanol [14,15] (Scheme 1). The ligands were satisfactorily characterized by elemental analyses, IR and ^{1}H NMR.

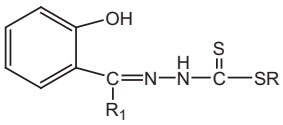

Keto (thione) form

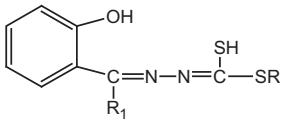

Enol (thiol) form

2.2.2. Syntheses of complexes

All the mononuclear MoO_2L complexes were prepared by refluxing $MoO_2(acac)_2$ and the respective ligands in dry methanol for 2 h. The complexes were satisfactorily characterized by elemental analyses, IR and ^{1}H NMR [14,15].

*2.2.2.1. (MoO_2L^1)$_2$(4,4′ bipy) (**1**).* A mixture of 0.856 g (2 mmol) of MoO_2L and 0.156 g (1 mmol) of 4,4′-bipyridine in dry methanol (20 mL) was refluxed for 3 h. The orange red crystalline compound was filtered, washed with dry methanol and dried in vacuo over anhydrous $CaCl_2$. Yield ~70%. *Anal.* Calc. for $C_{40}H_{32}N_6S_4O_6Mo_2$: C, 47.43; H, 3.16; N, 8.30; Mo, 18.97. Found: C, 46.88; H, 2.84; N, 8.34; Mo, 18.72%. IR (KBr Pellet) cm^{-1}: $\nu_{(C=N)}$ 1594 (vs), $\nu_{(Mo=O)}$ 980 (s), 895 (vs), $\nu_{(Mo-S)}$ 365 (m), $\nu_{(Mo-N)}$ 623 (m); UV–Vis (CH_2Cl_2) [λ_{max}/nm (ε/dm^3 mol^{-1} cm^{-1})]: 311 (7582), 395 (2907); ^{1}H NMR (dmso-d_6): (—S—CH_2—) 4.44 (s, 4H), (aromatic protons) 7.10–7.64 (m, 26H), (—CH=N) 8.97 (s, 2H).

*2.2.2.2. (MoO_2L^2)$_2$(4,4′ bipy) (**2**).* This complex is isolated when the same reaction is carried out in CH_2Cl_2 medium. *Anal.* Calc. for $C_{28}H_{24}N_6S_4O_6Mo_2$: C, 42.56; H, 2.79; N, 9.77; Mo, 22.32. Found: C, 42.35; H, 2.68; N, 9.72; Mo, 21.98%. IR (KBr Pellet) cm^{-1}: $\nu_{(C=N)}$ 1592 (vs), $\nu_{(Mo=O)}$ 975 (vs), 931 (vs), $\nu_{(Mo-S)}$ 363 (m), $\nu_{(Mo-N)}$ 633 (m); UV–Vis (CH_2Cl_2) [λ_{max}/nm (ε/dm^3 mol^{-1} cm^{-1})]: 241 (18037), 310 (8945), 398 (3306); ^{1}H NMR (dmso-d_6): (—S—CH_3) 2.66 (s, 6H), (aromatic protons) 7.23–7.67 (m, 16H), (—CH=N) 9.08 (s, 2H).

Complexes **2a**-**12** were prepared by refluxing the corresponding parent MoO_2L complex with 4,4′ bipyridine (4,4′ bipy), 1,2 bis (4-pyridyl) ethene, 1,2 bis (4-pyridyl) ethane in 2:1 M ratios in dry methanol for 3 h (Scheme 2). The orange red crystalline solids so formed were filtered, washed with dry methanol and dried in vacuo over anhydrous $CaCl_2$. Yield ~70–75%.

2.2.2.2a. (MoO_2L^2)$_2$(4,4′ bipy)(CH_3OH)$_2$ (**2a**). *Anal.* Calc. for $C_{30}H_{32}Mo_2N_6O_8S_4$: C, 38.93; H, 3.46; N, 9.08; Mo, 20.76. Found: C, 38.62; H, 3.35; N, 8.95; Mo, 20.58%. IR (KBr Pellet) cm^{-1}: $\nu_{(C=N)}$ 1596 (vs), $\nu_{(Mo=O)}$ 978 (s), 900 (vs), $\nu_{(Mo-S)}$ 365 (m), $\nu_{(Mo-N)}$ 625 (m); UV–Vis (CH_2Cl_2) [λ_{max}/nm (ε/dm^3 mol^{-1} cm^{-1})]: 317 (9512), 344 (4569); ^{1}H NMR (dmso-d_6): (—S—CH_3) 2.63 (s, 6H), (CH_3OH) 3.26 (s, 6H), (CH_3OH) 4.53 (s, 2H), (aromatic protons) 7.10–7.59 (m, 16H), (—CH=N) 8.92 (s, 2H).

*2.2.2.3. (MoO_2L^3)$_2$(4,4′ bipy) (**3**).* *Anal.* Calc. for $C_{42}H_{36}N_6S_4O_6Mo_2$: C, 48.46; H, 3.66; N, 8.07; Mo, 18.46. Found: C, 48.38; H, 3.35; N, 7.99; Mo, 17.86%. IR (KBr Pellet) cm^{-1}: $\nu_{(C=N)}$ 1572 (s), $\nu_{(Mo=O)}$ 998 (vs), 921 (vs), $\nu_{(Mo-S)}$ 380 (s), $\nu_{(Mo-N)}$ 561 (s); UV–Vis (CH_2Cl_2) [λ_{max}/nm (ε/dm^3 mol^{-1} cm^{-1})]: 296 (2042), 378 (7710); ^{1}H NMR (dmso-d_6):

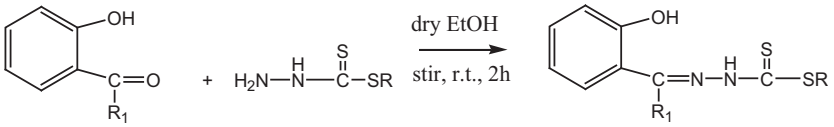

R	R_1	Ligand
$CH_2C_6H_5$	H	H_2L^1
CH_3	H	H_2L^2
$CH_2C_6H_5$	CH_3	H_2L^3
CH_3	CH_3	H_2L^4

Scheme 1. Reaction diagram for isolation of the ligands.

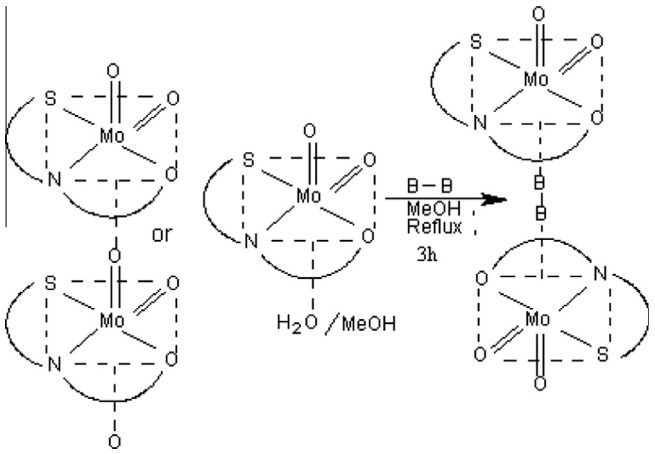

Scheme 2. Reaction diagram for the isolation of binuclear Mo(VI) complexes. [B-B = 4,4/bipyridine, 1,2 bis (4-pyridyl) ethene, 1,2 bis (4-pyridyl) ethane].

($H_3C—C_l=N—$) 2.79 (s, 6H), ($—S—CH_2—$) 4.45 (s, 4H), (aromatic protons) 6.89–7.90 (m, 26H).

*2.2.2.4. $(MoO_2L^4)_2$(4,4′ bipy) (**4**). Anal.* Calc. for $C_{30}H_{28}N_6S_4O_6Mo_2$: C, 40.54; H, 3.15; N, 9.46; Mo, 21.62. Found: C, 40.21; H, 3.00; N, 9.52; Mo, 21.32%. IR (KBr Pellet) cm^{-1}: $\nu_{(C=N)}$ 1580 (s), $\nu_{(Mo=O)}$ 935 (s), 900 (vs), $\nu_{(Mo-S)}$ 375 (m), $\nu_{(Mo-N)}$ 620 (m); UV–Vis (CH_2Cl_2) [λ_{max}/nm (ε/dm^3 mol^{-1} cm^{-1})]: 241 (13285), 271 (8165), 294 (8369), 370 (3222); ^{1}H NMR (dmso-d_6): ($—S—CH_3$) 2.58 (s, 6H), ($H_3C—C_l=N—$) 2.79 (s, 6H), (aromatic protons) 6.89–7.91 (m, 16H).

*2.2.2.5. $(MoO_2L^1)_2$ 1,2 bis (4-py) ethene (**5**). Anal.* Calc. for $C_{42}H_{34}N_6S_4O_6Mo_2$: C, 48.55; H, 3.27; N, 8.90; Mo, 18.49. Found: C, 48.43; H, 3.21; N, 8.69; Mo, 18.50%. IR (KBr Pellet) cm^{-1}: $\nu_{(C=N)}$ 1600 (vs), $\nu_{(Mo=O)}$ 974 (vs), 926 (vs), $\nu_{(Mo-S)}$ 362 (s), $\nu_{(Mo-N)}$ 634 (m); UV–Vis (CH_2Cl_2) [λ_{max}/nm (ε/dm^3 mol^{-1} cm^{-1})]: 285 (17200), 407 (3090); ^{1}H NMR (dmso-d_6): ($—S—CH_2—$) 4.41 (s, 4H), (Ar—CH=CH—Ar) 6.91–6.93 (d, 2H), (aromatic protons) 7.02–7.84 (m, 26H), (—CH=N) 8.99 (s, 2H).

*2.2.2.6. $(MoO_2L^2)_2$ 1,2 bis (4-py) ethene (**6**). Anal.* Calc. for $C_{30}H_{26}N_6S_4O_6Mo_2$: C, 40.63; H, 2.93; N, 9.48; Mo, 21.67. Found: C, 40.52; H, 2.89; N, 9.42; Mo, 21.51%. IR (KBr Pellet) cm^{-1}: $\nu_{(C=N)}$ 1600 (vs), $\nu_{(Mo=O)}$ 980 (vs), 925 (vs), $\nu_{(Mo-S)}$ 365 (m), $\nu_{(Mo-N)}$ 632 (m); UV–Vis (CH_2Cl_2) [λ_{max}/nm (ε/dm^3 mol^{-1} cm^{-1})]: 298 (14320), 403 (2580); ^{1}H NMR (dmso-d_6): ($—S—CH_3$) 2.55 (s, 6H), (Ar—CH=CH—Ar) 6.90–6.93 (d, 2H), (aromatic protons) 7.03–7.75 (m, 16H), (—CH=N) 8.90 (s, 2H).

*2.2.2.7. $(MoO_2L^3)_2$ 1,2 bis (4-py) ethene (**7**). Anal.* Calc. for $C_{44}H_{38}N_6S_4O_6Mo_2$: C, 49.53; H, 3.56; N, 7.88; Mo, 18.01. Found: C, 49.36; H, 3.48; N, 7.82; Mo, 17.95%. IR (KBr Pellet) cm^{-1}: $\nu_{(C=N)}$ 1600 (vs), $\nu_{(Mo=O)}$ 927 (vs), 900 (vs), $\nu_{(Mo-S)}$ 370 (m), $\nu_{(Mo-N)}$ 642 (m); UV–Vis (CH_2Cl_2) [λ_{max}/nm (ε/dm^3 mol^{-1} cm^{-1})]: 298 (20990), 382 (4610); ^{1}H NMR (dmso-d_6): ($H_3C—C_l=N—$) 2.76 (s, 6H), ($—S—CH_2—$) 4.42 (s, 4H), (Ar—CH=CH—Ar) 6.86–6.88 (d, 2H), (aromatic protons) 7.01–7.87 (m, 26H).

*2.2.2.8. $(MoO_2L^4)_2$ 1,2 bis (4-py) ethene (**8**). Anal.* Calc. for $C_{32}H_{30}N_6S_4O_6Mo_2$: C, 42.01; H, 3.28; N, 9.19; Mo, 21.00. Found: C, 42.00; H, 3.19; N, 8.98; Mo, 20.83%. IR (KBr Pellet) cm^{-1}: $\nu_{(C=N)}$ 1600 (vs), $\nu_{(Mo=O)}$ 925 (vs), 900 (vs), $\nu_{(Mo-S)}$ 368 (m), $\nu_{(Mo-N)}$ 635 (m); UV–Vis (CH_2Cl_2) [λ_{max}/nm (ε/dm^3 mol^{-1} cm^{-1})]: 290 (12060), 382 (2460); ^{1}H NMR (dmso-d_6): ($—S—CH_3$) 2.55 (s, 6H), ($H_3C—C_l=N—$) 2.76 (s, 6H), (Ar—CH=CH—Ar) 6.86–6.88 (d, 2H), (aromatic protons) 7.01–7.88 (m, 16H).

*2.2.2.9. $(MoO_2L^1)_2$ 1,2 bis (4-py) ethane (**9**). Anal.* Calc. for $C_{42}H_{36}N_6S_4O_6Mo_2$: C, 48.46; H, 3.46; N, 8.07; Mo, 18.46. Found: C, 48.26; H, 3.41; N, 8.10; Mo, 18.32%. IR (KBr Pellet) cm^{-1}: $\nu_{(C=N)}$ 1598 (vs), $\nu_{(Mo=O)}$ 975 (s), 898 (vs), $\nu_{(Mo-S)}$ 368 (m), $\nu_{(Mo-N)}$ 632 (m); UV–Vis (CH_2Cl_2) [λ_{max}/nm (ε/dm^3 mol^{-1} cm^{-1})]: 310 (4473), 393 (1721); ^{1}H NMR (dmso-d_6): ($Ar—CH_2—CH_2—Ar$) 2.96 (s, 4H), ($—S—CH_2—$) 4.40 s (4H), (aromatic protons) 6.90–7.56 (m, 26H), (—CH=N) 8.98 s (2H).

*2.2.2.10. $(MoO_2L^2)_2$ 1,2 bis (4-py) ethane (CH_3OH) (**10**). Anal.* Calc. for $C_{32}H_{36}N_6S_4O_8Mo_2$: C, 40.34; H, 3.78; N, 8.82; Mo, 20.17. Found: C, 40.32; H, 3.57; N, 8.62; Mo, 20.36%. IR (KBr Pellet) cm^{-1}: $\nu_{(C=N)}$ 1595 (vs), $\nu_{(Mo=O)}$ 976 (s), 900 (vs), $\nu_{(Mo-S)}$ 364 (m), $\nu_{(Mo-N)}$ 628 (m); UV–Vis (CH_2Cl_2) [λ_{max}/nm (ε/dm^3 mol^{-1} cm^{-1})]: 277 (7611), 315 (8467), 403 (2643); ^{1}H NMR (dmso-d_6): ($—S—CH_3$) 2.56 (s, 6H), ($Ar—CH_2—CH_2—Ar$) 2.92 (s, 4H), (CH_3OH) 3.31 (s, 3H), (CH_3OH) 4.46 (s, 2H) (aromatic protons) 6.90–7.55 (m, 16H), (—CH=N) 8.98 (s, 2H).

*2.2.2.11. $(MoO_2L^3)_2$ 1,2 bis (4-py) ethane (**11**). Anal.* Calc. for $C_{44}H_{40}N_6S_4O_6Mo_2$: C, 49.44; H, 3.74; N, 7.86; Mo, 17.98. Found: C, 49.37; H, 3.64; N, 7.82; Mo, 17.87%. IR (KBr Pellet) cm^{-1}: $\nu_{(C=N)}$ 1576 (s), $\nu_{(Mo=O)}$ 997 (vs), 899 (vs), $\nu_{(Mo-S)}$ 375 (m), $\nu_{(Mo-N)}$ 637 (m); UV–Vis (CH_2Cl_2) [λ_{max}/nm (ε/dm^3 mol^{-1} cm^{-1})]: 300 (9537), 381 (3669); ^{1}H NMR (dmso-d_6): ($H_3C—C_l=N—$) 2.76 (s, 6H), ($Ar—CH_2—CH_2—Ar$) 2.90 (s, 4H), ($—S—CH_2—$) 4.42 (s, 4H), (aromatic protons) 6.86–7.87 (m, 26H).

*2.2.2.12. $(MoO_2L^4)_2$ 1,2 bis (4-py) ethane (**12**). Anal.* Calc. for $C_{32}H_{32}N_6S_4O_6Mo_2$: C, 41.92; H, 3.49; N, 9.17; Mo, 20.96. Found: C, 42.00; H, 3.51; N, 9.13; Mo, 20.85%. IR (KBr Pellet) cm^{-1}: $\nu_{(C=N)}$ 1580 (s), $\nu_{(Mo=O)}$ 1000 (vs), 900 (vs), $\nu_{(Mo-S)}$ 378 (m), $\nu_{(Mo-N)}$ 634 (m); UV–Vis (CH_2Cl_2) [λ_{max}/nm (ε/dm^3 mol^{-1} cm^{-1})]: 298 (2577), 380 (9233); ^{1}H NMR (dmso-d_6): ($—S—CH_3$) 2.54 s (6H), ($H_3C—C_l=N—$) 2.76 s (6H), ($Ar—CH_2—CH_2—Ar$) 2.91 s (4H), (aromatic protons) 6.86–7.87 m (16H).

2.3. Physical measurements

Elemental analyses were performed on a Perkin-Elmer 240 C, H, N analyzer. NMR spectra were recorded on a Bruker 300 L NMR spectrometer operating at 300 MHz with TMS as internal standard. IR spectra were recorded as KBr pellets on a Perkin-Elmer model 883 infrared spectrophotometer. Electronic spectra were recorded using a HITACHI U-3501 UV–Vis recording spectrophotometer. Magnetic susceptibility was measured with a PAR model 155 vibrating sample magnetometer with Hg [$Co(SCN)_4$] as calibrant. Electrochemical data were collected on a Sycopel model AEW2 1820 F/S instrument at 298 K using a Pt working electrode, Pt auxiliary electrode and SCE reference electrode. Cyclic voltammograms were recorded in DMF containing 0.1 M TEAP as supporting electrolyte. Thermal analyses were carried out in a Mettler Toledo TGA/SDTA 851 thermal Analyzer in a dynamic atmosphere of dinitrogen (flow rate = 30 cm^3 min^{-1}).

2.4. Computational details

Full geometry optimization of **2**, **2a**, **9** and **10** were carried out using the DFT method at the B3LYP level of theory [16,17]. The 6–31+G(d) basis set was assigned for all elements except molybdenum. The LanL2DZ basis set with effective core potential was employed for the molybdenum atom [18–20]. The vibrational frequency calculations were performed to ensure that the optimized

geometries represent the local minima of potential energy surface and there are only positive eigen-values. The lowest 50 singlet–singlet vertical electronic excitations based on B3LYP optimized geometries were computed using the time-dependent density functional theory (TDDFT) formalism [21–23] in CH_2Cl_2 using the conductor-like polarizable continuum model (CPCM) [24–26] with B3LYP and the above basis sets. All computations were performed using the GAUSSIAN09 and GAUSSIAN03 programs [27]. GAUSSSUM [28] was used to calculate the fractional contributions of various groups to each molecular orbital.

2.5. Crystallographic measurements

The crystallographic data for complex **2** was collected on an Oxford Diffaction X-Calibur System, for complexes **2a** and **9** on a Siemens P4 4-circle-diffractometer and for complex **10** was collected on a Bruker APEX-II diffractometer with CCD-area detector. All data sets were obtained with graphite-monochromated Mo Kα (λ = 0.71073 Å) radiation. Unit-cell dimension and intensity data for **2**, **2a**, **9**, **10** were measured at 150(2), 294(2), 294(2) and 296(2) K respectively. The crystal structures were solved by direct methods using SHELXS-97 and refined by full-matrix least-squares based on F^2 with anisotropic displacement parameter of non-hydrogen atoms using SHELXL-97. The hydrogen atoms were included in calculated positions. The ligand in **2** was completely disordered over a pseudo mirror plane containing atoms Mo(1), O(1) and O(2), each atom occupying two possible sites. The structure was refined using occupation factors that converged to 0.67(1) and 0.33(1) respectively.

3. Results and discussion

3.1. Synthesis

The Schiff base ligands (H_2L^1, H_2L^2, H_2L^3 and H_2L^4) were prepared by condensing S-benzyl and S-methyl dithiocarbazates with salicylaldehyde and 2-hydroxyacetophenone in ethanol. The ligands were satisfactorily characterized by elemental analyses, IR and ^{1}H NMR.

All the binuclear complexes (**1**–**12**) of general formula $[(MoO_2L)_2(B\text{-}B)]$ were prepared by refluxing the corresponding parent MoO_2L complex with 4,4′ bipyridine (4,4′ bipy), 1,2 bis (4-pyridyl) ethene and 1,2 bis (4-pyridyl) ethane in 2:1 M ratios in dry methanol.

All the orange yellow Mo(VI) binuclear complexes (**1**–**12**) are air stable in the solid state. The compounds are readily soluble in alcohol, CH_2Cl_2, CH_3CN, DMF and DMSO but are insoluble in water. The complexes are diamagnetic at room temperature as is expected for d°Mo(VI) centers [29]. Molar conductivity data in 10^{-3}M CH_2Cl_2 solution indicate that they are non-electrolytes. All the binuclear Mo(VI) complexes are satisfactorily characterized by elemental analyses, IR, ^{1}H NMR, electronic spectra and cyclic voltammetric data. The complexes **2**, **2a**, **9** and **10** have been structurally characterized by single crystal X-ray diffraction. DFT calculations on the ligand and complexes **2**, **2a**, **9** and **10** were also carried out.

3.2. Spectral characteristics

Characteristic IR bands of binuclear molybdenum(VI) complexes are given in Section 2.2.2. A strong ν(C=N) band [30,31] was observed around 1572–1600 cm^{-1} region for the complexes. A new band in the 561–642 cm^{-1} region was observed for complexes and is assigned to the ν(Mo—N) [32,33]. The complexes exhibit a medium intensity band around 362–380 cm^{-1} which may be assigned to ν(Mo—S) [34]. Two IR bands are observed in the 1000–895 cm^{-1} region, the higher frequency band originating from the anti-symmetric while the lower one from the symmetric stretching mode of the $[MoO_2]^{2+}$moiety [32,35,36].

^{1}H NMR data for the ligands and the corresponding complexes (**1**–**12**) are summarized in Sections 2.2.1 and 2.2.2. The relative broad signals at δ 10.72 and 10.02 ppm; δ 10.24 and 10.09 ppm; δ 11.25 and 11.26 ppm; δ 11.42 and 12.68 ppm in the ^{1}H NMR spectra corresponding to O—H and N—H of the ligands H_2L^1, H_2L^2, H_2L^3 and H_2L^4 disappear in the complexes **1**–**12** as a result of complexation. The signals at δ 8.04 and 8.01 ppm of the ligand have shifted downfield to δ 8.97; 8.92; 8.98; 8.91; 8.99 and 8.91 ppm indicating coordination from the azomethine nitrogen in the complexes **1**, **2**, **5**, **6**, **9** and **10**. In the complexes **3**, **4**, **7**, **8**, **11** and **12**, the involvement of the azomethine nitrogen is indicated by the shift of the $-CH_3$ proton signal from δ 2.47 to 2.79, 2.76 and δ 2.46 to 2.79, 2.76 ppm respectively. The methylene protons of the ligands and the complexes **1**, **3**, **5**, **7**, **9** and **11** appearing at δ 4.59, 4.51, 4.44, 4.45, 4.40, 4.42, 4.41 and 4.42 ppm respectively indicate that the S-benzyl sulfur is not involved in the coordination. The nine aromatic protons appear as multiplets within the range δ 7.24–7.43 (7H), δ 6.92–6.98 (2H) and δ 7.24–7.431 (7H), δ 6.64–6.90 (2H) ppm for the ligands H_2L^1 and H_2L^3 respectively. In complexes **1**, **3**, **5**, **7**, **9** and **11** twenty-six aromatic protons appear as multiplets within the range δ 7.10–7.64, δ 6.89–7.90, δ 6.90–7.56, δ 6.86–7.89, δ 7.02–7.84, δ 7.01–7.87 ppm respectively.

Similar observations for aromatic protons have been made with the ligands H_2L^2 and H_2L^4 and their corresponding complexes. The methyl protons of the ligands H_2L^2 and H_2L^4 and their complexes appear at nearly the same positions. Considering IR and ^{1}H NMR data together, it is clear that results are consistent in describing the donor sites of the ligands bound to the $[MoO_2]^{2+}$ center.

Electronic spectra of the binuclear molybdenum(VI) complexes were recorded in dry dichloromethane and the spectral data of complexes are presented in the Section 2.2.2. Spectra of all the binuclear $[(MoO_2L)_2$ (B-B)] complexes exhibit several bands in the 407–241 nm range. The absorption maxima are located in the 400–300 nm range and may be assigned [37] to S($p\pi$)—Mo($d\pi$) LMCT transition caused by the promotion of an electron from the filled HOMO of the ligand of primarily sulfur $p\pi$ character to the empty LUMO of molybdenum $d\pi$ character. Other LMCT bands are observed in the region 300–277 nm [31,38–40]. The bands appearing below 277 nm are due to intra-ligand transitions.

3.3. Electrochemical properties

Cyclic voltammograms of the binuclear molybdenum(VI) complexes (**1**–**12**) at a platinum electrode were recorded in dry degassed DMF containing 0.1 M TEAP as the supporting electrolyte

Table 1
Cyclic voltammetric results[a] (V vs. SCE) for the $[(Mo^{VI}O_2L)_2(B\text{-}B)]$ complexes at 298 K.

Complexes	E_{pc} (V)	E_{pa} (V)
$(MoO_2L^1)_2$(4,4′ bipy) (**1**)	−1.22	+0.68
$(MoO_2L^2)_2$(4,4′ bipy) (**2**)	−1.16	+0.64
$(MoO_2L^2)_2$(4,4′ bipy)$(CH_3OH)_2$ (**2a**)	−1.12	+0.65
$(MoO_2L^3)_2$ (4,4′ bipy) (**3**)	−1.18	+0.68
$(MoO_2L^4)_2$ (4,4′ bipy) (**4**)	−1.09	+0.65
$(MoO_2L^1)_2$ 1,2,bis(4-py)ethene (**5**)	−1.10	+0.69
$(MoO_2L^2)_2$ 1,2,bis(4-py)ethene (**6**)	−1.09	+0.67
$(MoO_2L^3)_2$ 1,2,bis(4-py)ethene (**7**)	−1.15	+0.67
$(MoO_2L^4)_2$ 1,2,bis(4-py)ethene (**8**)	−1.15	+0.68
$(MoO_2L^1)_2$1,2,bis(4-py)ethane (**9**)	−1.10	+0.90
$(MoO_2L^2)_2$ 1,2,bis(4-py)ethane (**10**)	−1.08	+0.99
$(MoO_2L^3)_2$ 1,2,bis(4-py)ethane (**11**)	−1.16	+0.69
$(MoO_2L^4)_2$ 1,2,bis(4-py)ethane (**12**)	−1.17	+0.73

[a] *Solvent:* DMF (dry, degassed); supporting electrolyte: 0.1 M TEAP; solution strength: 10^{-3} M; working electrode: platinum; reference electrode: SCE: 100 mV s^{-1}.

over a potential range of 0.0 to −1.5 V. Results of cyclic voltammetric studies of all the binuclear Mo(VI) complexes are presented in Table 1 and the representative diagrams are shown in Fig. S1. The complexes (**1**–**12**) exhibit only one irreversible two electron one step reduction within the potential window −1.08 to −1.22 V region versus SCE in DMF solution which are assigned to Mo^{VI}–Mo^{VI}/Mo^{IV}–Mo^{IV} process [31,38,40]. A two-electron involvement is established by a comparison of the current height with authentic two electron species under identical experimental condition. On scan reversal, one irreversible two-electron oxidative response is located in the 0.64 to 0.99 V range. It is to be noted that the reduction of binuclear dioxo Mo(VI) complexes in aprotic solvents is generally irreversible.

3.4. Thermal properties of complex *2a*

The TG/DTA study of complex **2a** was conducted in the temperature range of 30–600 °C with a 10 °C/min temperature interval in nitrogen atmosphere. Above 200 °C, the TG/DTA curve exhibits three steps of weight losses. The compound starts losing weight by an exothermic peak around 246 °C in the TG/DTA curve due to the concomitant removal of two CH_3OH molecules and the bridging 4,4′-bipyridyl molecule. Step-1 is reasonable as the 4,4′-bipyridyl moiety is attached to the two mononuclear units MoO_2CH_3OH through the coordinated methanol and should be removed with the loss of two CH_3OH molecules which hold it through hydrogen bonding. In the second step, the loss of the CH_3—S—S—CH_3 moiety is suggested by an exothermic peak around 280 °C in the DTA curve. It can be attributed to the fact that at 280 °C, the stable CH_3—S—S—CH_3 species is eliminated rather than the more reactive species CH_3–S species. The compound finally changes into stable MoO_3 at 570 °C. The observed loss of weights corroborates the proposed decomposition processes.

3.5. Study of reactivity

All the binuclear dioxo Mo(VI) complexes exhibit oxo-transfer to the substrate PPh_3, when reacted with PPh_3 in 1:1.5 M proportions in dry CH_3CN medium. The oxo-transfer reaction may be represented as

$$[(MoO_2L)_2(B\text{-}B)] + 2PPh_3 \xrightarrow{CH_3CN} 2MoOL(B\text{-}B) + 2\,OPPh_3$$

When the brown solution of Mo(IV) complexes in CH_3CN is reacted with DMSO or pyridine N-oxide, the brown color of the solution gradually changes to orange indicating oxo-transfer from the substrate DMSO or pyridine N-oxide to the mono oxo $[MoO]^{2+}$ center to regenerate the parent $[MoO_2]^{2+}$ species.

$$MoOL(B\text{-}B) + DMSO \xrightarrow{CH_3CN} MoO_2L + B\text{-}B + Me_2S$$

3.6. Description of the crystal structures of complexes *2*, *2a*, *9* and *10*

The molecular structure and the atom numbering scheme of complexes **2**, **2a**, **9** and **10** are shown in Figs. 1–4. Crystallographic data and selected bond lengths and bond angles are presented in Tables 2 and 3 respectively.

The orange binuclear complex **2** contains a crystallographic center of inversion. Structural equivalence of the two Mo(VI) centers is reflected in the simultaneous electrochemical reductions of the two Mo(VI) centers at the same potential. Each Mo(1) is bonded to two oxo atoms, O, N and S donor atoms of the ligand H_2L^2 and one nitrogen atom of the bridging 4,4′ bipyridine molecule in a distorted octahedral coordination environment around the metal center. Dimensions from the major component of the disordered ligand will be discussed. Two Mo-atoms (Mo—Mo distance = 11.957 Å) are linked by two bridged nitrogen atoms of 4,4′-bipyridine. The ligand is active in its enolate form and behaves in a dianionic tridentate manner. The three donor points O(11), N(3), S(1) of the ligand and one terminal oxygen O(2) occupies a meridonial plane [41,42]. The dianionic tridentate ligand forms one five membered and another six membered chelating ring around the $[MoO_2]^{2+}$ center with bite angles of N(3)—Mo(1)—S(1),72.6(3)° and O(11)—Mo(1)—N(3), 82.2(4)°. The other oxo-oxygen O(2) occupies an apical position in the coordination sphere of Mo(1). The Mo(VI) center is slightly displaced by 0.375(3) Å from the equatorial plane in the direction of the terminal oxygen atom O(1). The other apical position is occupied by the nitrogen atom N(41) of one half of the 4,4′ bipy unit. The Mo(1)—N(41) bond length [2.435(7) Å] is considerably longer than the other Mo(1)—N(3) bond [2.321(11) Å], no doubt because of the trans influence of O(1), a value which indicates that the bipyridine nitrogen is comparatively weakly bonded to the $[MoO_2]^{2+}$ core pointing to the possibility of ligand exchange reaction at this point.

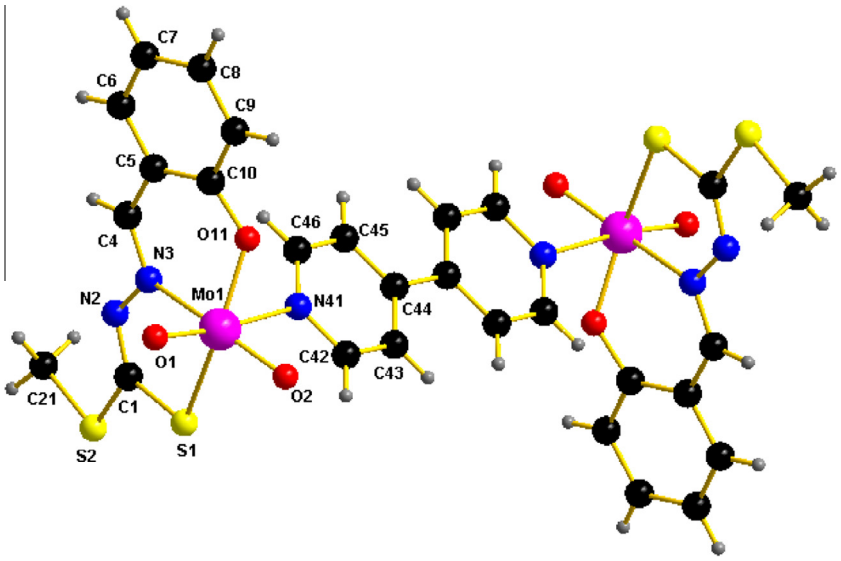

Fig. 1. Molecular structure of complex $(MoO_2L^2)_2$(4,4′ bipy) (**2**).

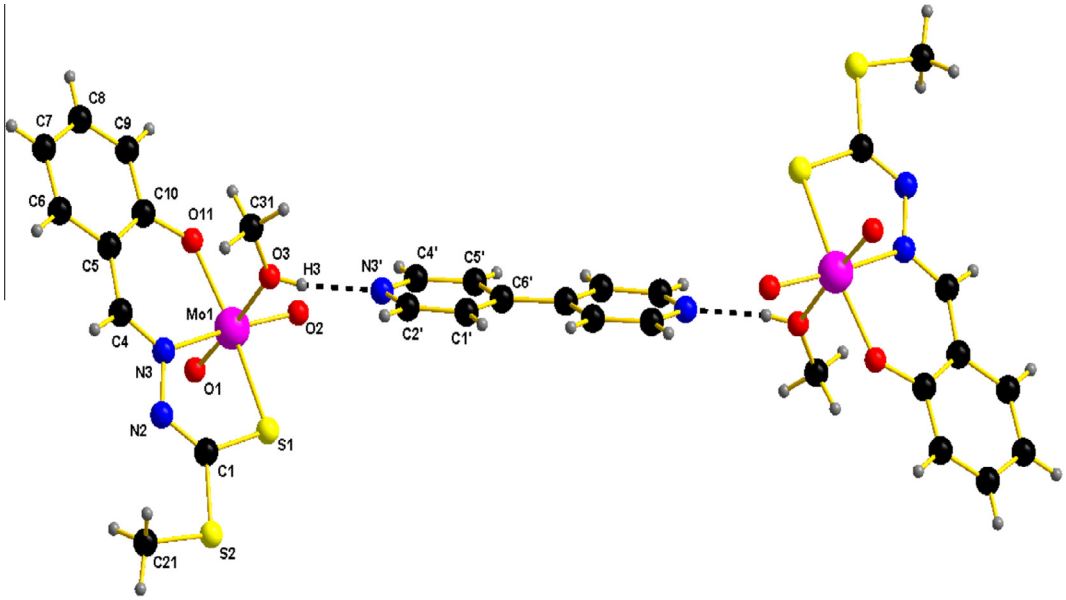

Fig. 2. Molecular structure of complex $(MoO_2L^2)_2(4,4'\ bipy)(CH_3OH)_2$ (**2a**).

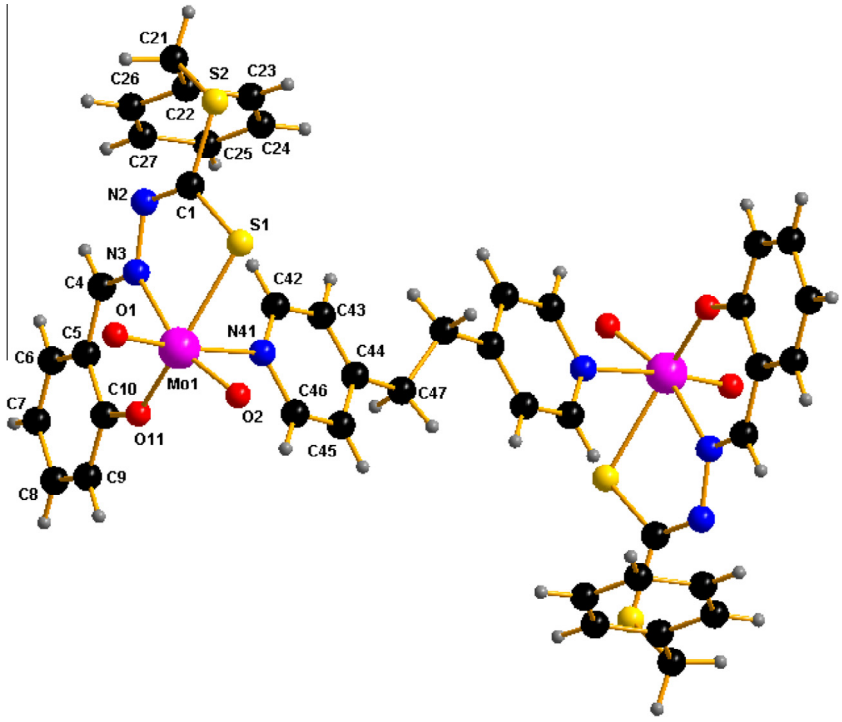

Fig. 3. Molecular structure of complex $(MoO_2L^1)_2$ 1,2 bis (4-py) ethane (**9**).

Due to coordination in the thiolate form of the ligand, the C(1)—S(1) bond is expected to assume a single bond character but in the complex, the length is 1.78(2) Å which lies between the length of C—S bond and C=S bond and may be attributed to electron delocalization in the coordinated ligand [43,44]. The adjacent C(1)—N(2) bond length is 1.26(2) Å and is closer to the C=N distance than the normal C—N distance. The N(2)—N(3) bond distance of 1.38(2)Å reveals its predominant single bond character. Two types of intermolecular hydrogen bonding interactions (Fig. S2) are observed between O(1) and H(43) with bond lengths O(1)···H(43) 2.57 Å, O(1)···C(43) 3.230 Å and bond angle O(1)···H(43)—C(43) 128° and S(2) and H(43) with bond lengths S(2)···H(43) 3.10 Å, S(2)···C(43) 3.91 Å and bond angle S(2)···H(43)—C(43) 145.95°. The O···H interactions lead to the formation of chain like architecture and the adjacent chains are interconnected through the S···H hydrogen bonds. The packing diagram for complex **2** is shown in Fig. 5.

In the case of complex **2a**, also centrosymmetric, instead of direct bonding of the two nitrogen atoms of 4,4′-bipyridine molecule to the vacant sixth position of Mo(VI) as in complex **2**, the ligand is attached to the bonded methanol molecule through a strong hydrogen bond [O(3)—H(3)···N(3′)] (Fig. 2) involving the

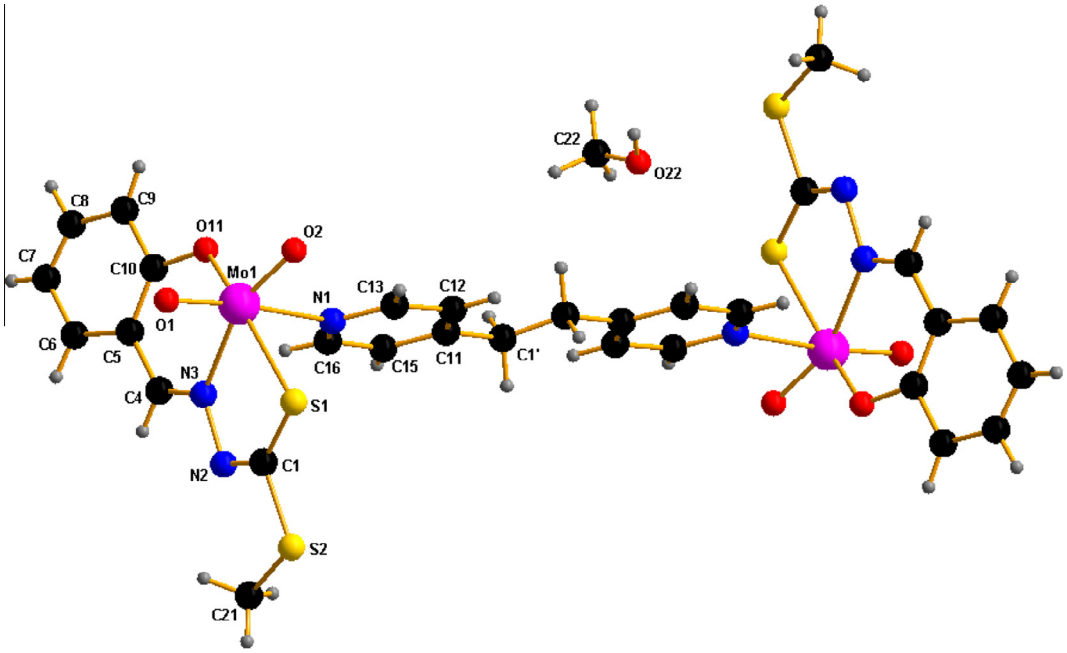

Fig. 4. Molecular structure of complex $(MoO_2L^2)_2$ 1,2 bis (4-py) ethane (**10**).

Table 2
Crystal data and details of refinement for complexes **2**, **2a**, **9** and **10**.

	Complex **2**	Complex **2a**	Complex **9**	Complex **10**
Chemical formula	$C_{28}H_{24}Mo_2N_6O_6S_4$	$C_{30}H_{32}Mo_2N_6O_8S_4$	$C_{42}H_{36}Mo_2N_6O_6S_4$	$C_{32}H_{36}Mo_2N_6O_8S_4$
Formula weight (M)	860.66	924.74	1040.89	952.79
Crystal system	monoclinic	monoclinic	triclinic	trigonal
Space group	$P2_1/n$	$P2_1/n$	$P\bar{1}$	$R\bar{3}$
a (Å)	9.743(2)	7.0612(14)	9.1780(18)	22.9640(17)
b (Å)	12.052(4)	17.701(4)	10.450(2)	22.9640(17)
c (Å)	14.434(3)	14.898(3)	12.383(3)	18.8337(14)
α (°)	90	90	79.92(3)	90
β (°)	96.53(2)	100.24(3)	74.63(3)	90
γ (°)	90	90	72.69(3)	120
V (Å^3)	1683.9(8)	1832.5(6)	1087.3(4)	8601.2(11)
Z	2	4	1	9
T (K)	150(2)	294(2)	294(2)	296(2)
D_C (g cm^{-3})	1.697	1.676	1.590	1.655
μ (Mo Kα) (mm^{-1})	1.043	0.968	0.823	0.931
F(000)	860	932	526	4338
Goodness of fit (GOF) on F^2	0.916	1.016	0.937	1.171
R_1, wR_2 $[I > 2\sigma(1)]$	R_1 = 0.0933, wR_2 = 0.2205	R_1 = 0.0444, wR_2 = 0.0779	R_1 = 0.0894, wR_2 = 0.1632	R_1 = 0.1209, wR_2 = 0.2454

—OH hydrogen atom of the coordinated methanol, with O···N 2.646(8), H···N 1.886 Å and O—H···N angle 171°. Complex **2a** is further stabilized via π-π stacking interactions which are facilitated by the electron withdrawing N atom in the bipyridine moiety which decreases the π-electron repulsion by reducing the π-electron density in the ring. Fig. 6 shows the π-π stacking interactions, centroid–centroid distance 3.499 Å with perforce parallel rings, a distance comparable to previously reported π-π stacking interactions [45]. The Mo—Mo distance in complex **2a** (14.890 Å) is much longer than the Mo—Mo distance in complex **2** (11.958 Å) due to different types of interaction of the spacer with the Mo-centers in the two cases. In complex **2a**, the Mo(VI) center is slightly displaced by 0.303 Å from the mean equatorial plane described by O(2),S(1),N(3) and O(11) towards the apical oxo-oxygen O(1).

In complex **9** which is also centrosymmetric the Mo—Mo distance is 14.383 Å and the two Mo centers are linked by two bridging N atoms of 1,2-bis(4-py)ethane moiety. The Mo(VI) center is present in a distorted donor environment consisting of two *cis* oxo atoms O(1) and O(2), phenolate oxygen O(11), thioenolate sulfur S(1), azomethine nitrogen N(3) and nitrogen atom N(41) of one half of the 1,2-bis (4-py)ethane unit.

The addition of 1,2-bis (4-py)ethane to the vacant position trans to the oxo atom O(1) generates an O(1)—Mo(1)—N(41) angle of 169.9(3)°. The Mo center is slightly displaced by 0.323 Å from the equatorial plane towards the apical oxo oxygen O(1).

In the crystal packing structure (Fig. S3) of complex **9**, an intermolecular hydrogen bond was observed between the oxo atom O(1) and H(25) (1 + x, y, z) (a ring hydrogen atom of the S-benzyl moiety of the ligand) with dimensions O···H 2.81 Å, O···C 3.620 Å and angle O···H—C 146° (Fig. S4). The hydrogen bonding pattern thus gives rise to a ladder like architecture along the a-direction. The hydrogen bond dimensions are consistent with previously reported values [46].

Complex **10** is also centrosymmetric. The coordination geometry around the Mo(VI) center is distorted octahedral. Here, the Mo centers are linked by 1,2-bis(4-py)ethane moiety, the Mo—Mo

Table 3
Experimental and calculated dimensions in **2**, **2a**, **9** and **10** with distances (Å) and angles (deg).

	Complex **2**		Complex **2a**		Complex **9**		Complex **10**	
Bond distances(Å)	obs[a]	calc	obs	calc	obs	calc	obs	calc
Mo(1)–O(1)	1.715(6)	1.710	1.707(2)	1.709	1.677(7)	1.711	1.694(10)	1.711
Mo(1)–O(2)	1.695(6)	1.720	1.711(2)	1.725	1.724(7)	1.720	1.711(10)	1.720
Mo(1)–S(1)	2.548(4)	2.477	2.444(1)	2.476	2.451(3)	2.480	2.481(5)	2.480
Mo(1)–O(11)	1.863(8)	1.975	1.956(2)	1.970	1.930(8)	1.973	2.042(16)	1.977
Mo(1)–N(3)	2.321(11)	2.337	2.277(3)	2.328	2.286(8)	2.334	2.278(14)	2.338
Mo(1)–N(41)[b]	2.435(7)	2.504	–	–	2.456(8)	2.509	2.443(13)	2.513
N(2)–N(3)	1.375(18)	1.332	1.423(3)	1.382	1.412(11)	–	1.468(17)	1.383
Bond angles (°)								
O(1)–Mo(1)–O(2)	105.6(3)	106.5	105.3(1)	106.4	1.677(7)	1.771	106.0(5)	106.5
O(1)–Mo(1)–O(11)	102.5(4)	99.7	98.3(1)	99.8	1.930(8)	1.973	96.1(6)	99.3
O(1)–Mo(1)–N(3)	92.9(3)	92.4	92.4(1)	92.7	92.3(3)	92.6	92.5(5)	92.2
O(1)–Mo(1)–S(1)	99.0(3)	101.2	96.1(1)	98.6	96.8(3)	99.6	100.1(4)	100.9
O(1)–Mo(1)–N(41)[b]	170.5(3)	172.6	–	–	169.9(3)	172.5	169.7(5)	172.1
O(2)–Mo(1)–O(11)	104.6(4)	106.4	104.6(1)	105.4	102.9(3)	104.3	103.8(5)	106.6
O(2)–Mo(1)–N(3)	158.1(3)	158.2	159.4(1)	158.3	158.9(3)	158.6	158.7(5)	158.3
O(2)–Mo(1)–S(1)	92.6(3)	90.6	91.0(1)	88.8	91.6(3)	92.1	90.4(4)	90.6
O(2)–Mo(1)–N(41)[b]	83.9(3)	80.6	–	–	83.8(3)	81.0	84.1(5)	81.1
O(11)–Mo(1)–N(3)	82.2(4)	80.3	82.9(1)	81.0	83.3(3)	81.0	84.2(5)	81.3
O(11)–Mo(1)–S(1)	147.5(3)	148.0	155.1(1)	152.1	153.6(2)	151.4	154.6(4)	151.4
O(11)–Mo(1)–N(41)[b]	75.2(3)	76.1	–	–	78.6(3)	77.0	79.5(5)	74.9
N(3)–Mo(1)–S(1)	72.6(3)	74.9	76.4(1)	75.1	75.9(3)	75.0	75.7(4)	74.9
N(3)–Mo(1)–N(41)[b]	77.7(3)	81.0	–	–	77.6(3)	80.1	77.9(5)	80.7
S(1)–Mo(1)–N(41)[b]	79.5(2)	80.3	–	–	81.2(2)	–	81.2(3)	80.6

[a] Dimensions from the ligand positions with the highest occupancy.
[b] This atom is N(41) in 2, 2a and 9 but N(1) in 10.

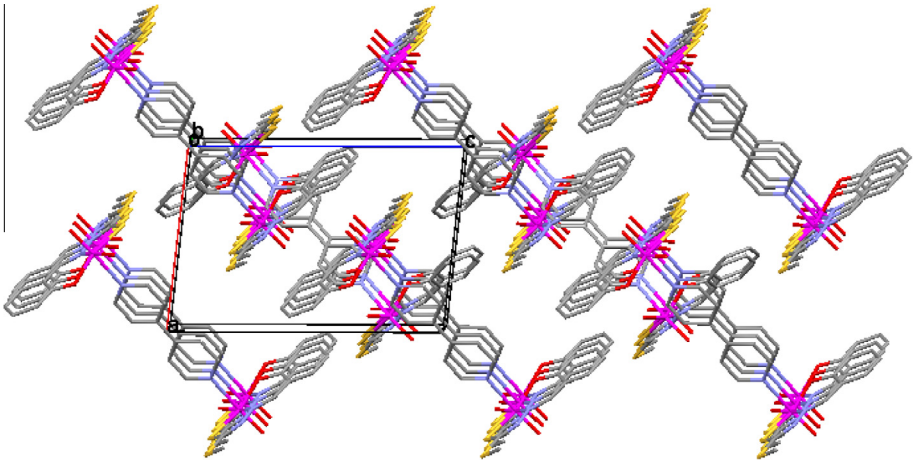

Fig. 5. Packing diagram for complex **2** around the *b* axis, hydrogen atoms are omitted for clarity.

distance being 14.245 Å. Here the metal atom is 0.326 Å away from the equatorial plane in the direction of the terminal oxygen atom O(1). Six binuclear moieties along with six floating methanol molecules together form a cylindrical cavity as shown in Fig. 7. The cavity is basically formed by three overlapping rings of hydrogen bonds. The ring in the middle is formed by six hydrogen bonded methanol molecules. Two types of hydrogen bonding interactions are responsible for such an interesting supramolecular architecture–C(31)—H(31A)···O(31) with hydrogen bond length 1.813 Å, angle 107.10° and C(21)—H(21B)···(S2) with hydrogen bond length 3.181 Å, angle 132.43°. Hydrogen bonds involving sulfur atoms are comparatively longer than those involving N or O because of the larger size of sulfur and its more diffuse electron cloud [47]. The top view (along the *c*-axis) shows that a star shaped cavity (Fig. S5) is formed which may be used to trap other suitable ions [48]. In 3-D, the packing structure appears as a sheet of fused six-membered rings with each ring having a cavity (Fig. S6).

It is to be noted that the structural features of each of the two units of the binuclear complexes **2**, **2a**, **9** and **10** are closely similar to those of their precursor mononuclear complex MoO_2L and remind us of the situation when a substrate binds itself at the active center of a metalloenzyme. In that case also, the major structural characteristic of the enzyme remains almost unaltered.

*3.7. DFT and TD-DFT calculations of ligands and complexes **2**, **2a**, **9** and **10***

The full geometry optimizations of **2**, **2a**, **9** and **10** were carried out using the DFT/B3LYP method. The calculated bond parameters are compared to experimental values in Table 3 and show good agreement. For complex **2** the maximum deviation in bond length is Mo(1)—O(11) 0.112 Å, for **2a** N(2)—N(3) 0.041 Å, for **9** Mo(1)—N(41) 0.053 Å and N(2)—N(3) 0.085 Å for complex **10**.

In complex **2a**, the computed value (1.822 Å) for the hydrogen bond distance [H(3)···N(3′)] is in good agreement with the experimental value (1.886 Å), the maximum deviation being ~0.064 Å.

The compositions along with the energies of some selected molecular orbitals of complexes are given in Tables 4–7. Contour

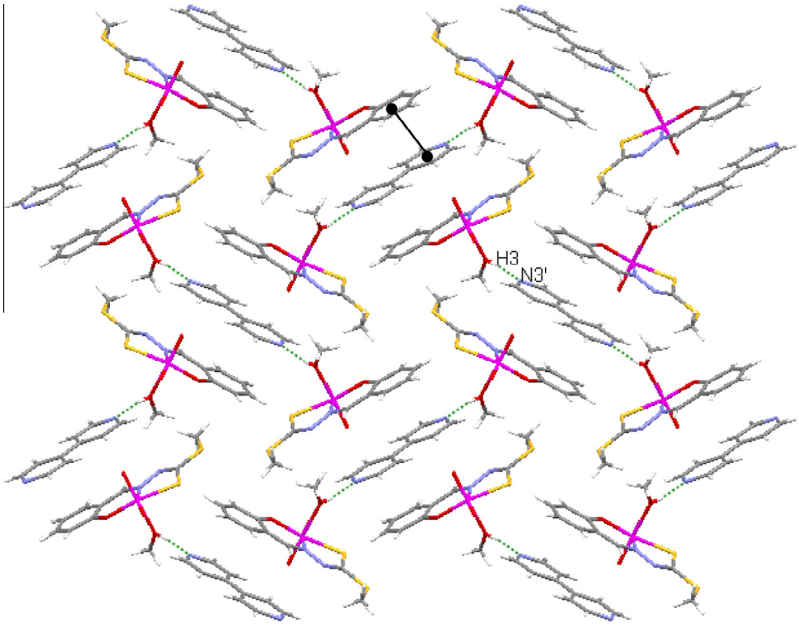

Fig. 6. Packing diagram for complex **2a** around the a axis showing the hydrogen-bonding (1.886Å) between N(3′) and H(3) (the hydrogen bond is represented as a green dashed line) and the intermolecular π-π stacking interactions (3.499 Å) (the π-π stacking interaction is represented as a black straight line). (Colour online.)

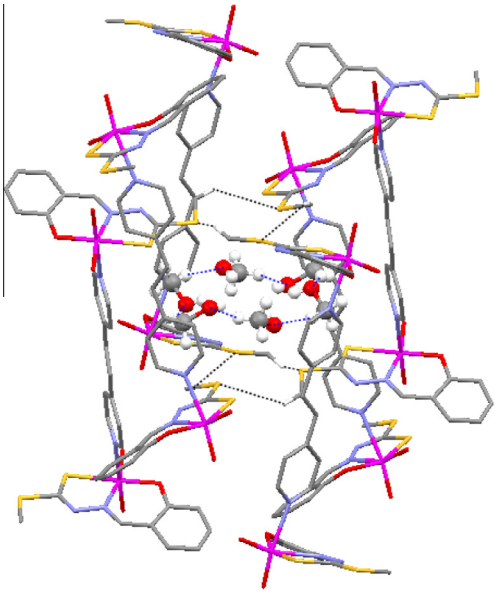

Fig. 7. Diagram for complex **10** illustrating the formation of a cylindrical cavity as a result of two types of hydrogen bonding interactions (H(31A)···O(31) = 1.813 Å (the hydrogen bond is represented as a blue dashed line) and H(21B)···(S2) = 3.181 Å (the hydrogen bond is represented as a black dashed line)). (Colour online.)

plots of some selected frontier molecular orbitals of the complexes are shown in Figs. 8–11. As the molecules are centerosymmetric, only HOMO, HOMO−2, LUMO and LUMO+2 are given. The higher energy occupied molecular orbitals (HOMO to HOMO−5) have ligand (L) contribution with 57–67% $p\pi$(S) contribution in HOMO−2 and HOMO−3. For complexes **2** and **2a**, the low energy unoccupied molecular orbitals (LUMO to LUMO+3 and LUMO+5) have $d\pi$(Mo) and π^*(L) character along with minor contributions of $p\pi$(O) orbital, while LUMO+4 has π^*(bpy) character. Similarly for complexes **9** and **10** the LUMO to LUMO+5 have $d\pi$(Mo), π^*(L) and $p\pi$(O) character.

To investigate the electronic spectra of the complexes vertical electronic excitations have been calculated by the TDDFT/CPCM method in CH_2Cl_2 solvent. The calculated excitation wavelength

Table 4
Energy and composition of selected molecular orbitals of complex **2**.

MO	Energy (eV)	% of composition			
		Mo	L	bpy	Oxo
LUMO+5	−2.01	24	67	01	09
LUMO+4	−2.29	06	15	76	03
LUMO+3	−2.50	58	21	0	21
LUMO+2	−2.50	57	20	01	21
LUMO+1	−2.68	39	37	05	19
LUMO	−2.74	34	30	17	19
HOMO	−6.11	01	96 ($p\pi$S), 27)	02	01
HOMO−1	−6.12	01	95 ($p\pi$(S), 26)	02	02
HOMO−2	−6.64	01	91 ($p\pi$(S), 66)	03	05
HOMO−3	−6.66	01	92 ($p\pi$(S), 63)	01	05
HOMO−4	−6.70	0	98 ($p\pi$(S), 32)	01	01
HOMO−5	−6.71	0	98 ($p\pi$(S), 39)	02	0
HOMO−6	−7.41	03	81	03	14
HOMO−7	−7.42	03	80	03	14
HOMO−8	−7.72	0	90	08	02
HOMO−9	−7.72	0	91	07	02
HOMO−10	−7.87	03	23	58	23

Table 5
Energy and composition of selected molecular orbitals of complex **2a**.

MO	Energy (eV)	% of composition				
		Mo	L	oxo	MeOH	bpy
LUMO+5	−1.80	25	65	11	0	0
LUMO+4	−2.11	0	0	0	0	99
LUMO+3	−2.39	59	21	21	0	0
LUMO+2	−2.41	59	19	21	0	0
LUMO+1	−2.49	42	35	22	0	0
LUMO	−2.51	42	37	22	0	0
HOMO	−5.92	01	97($p\pi$ (S), 28)	01	01	0
HOMO−1	−5.94	01	96($p\pi$ (S), 27)	01	01	01
HOMO−2	−6.46	01	92($p\pi$ (S), 66)	06	01	0
HOMO−3	−6.49	01	92($p\pi$ (S), 57)	06	01	0
HOMO−4	−6.54	0	99($p\pi$ (S), 34)	0	01	0
HOMO−5	−6.56	01	98($p\pi$ (S), 43)	0	01	0
HOMO−6	−7.22	03	83	13	01	0
HOMO−7	−7.24	03	83	13	01	0
HOMO−8	−7.52	01	13	21	63	03
HOMO−9	−7.52	01	14	21	63	02
HOMO−10	−7.54	0	90	03	06	01

Table 6
Energy and composition of selected molecular orbitals of complex **9**.

MO	Energy (eV)	% of composition			
		Mo	L	Oxo	brid
LUMO+5	−1.91	25	64	10	01
LUMO+4	−1.92	24	65	10	01
LUMO+3	−2.50	57	19	23	0
LUMO+2	−2.50	58	19	23	0
LUMO+1	−2.65	37	42	20	01
LUMO	−2.65	38	41	20	01
HOMO	−6.02	01	96($p\pi$(S), 26)	01	02
HOMO−1	−6.03	01	96($p\pi$ (S), 26)	01	02
HOMO−2	−6.56	01	92($p\pi$ (S), 65)	05	02
HOMO−3	−6.56	01	92($p\pi$ (S), 67)	04	02
HOMO−4	−6.63	0	98($p\pi$ (S), 17)	01	01
HOMO−5	−6.64	0	99($p\pi$ (S), 19)	01	0
HOMO−6	−7.00	01	97($p\pi$ (S), 17)	01	01
HOMO−7	−7.01	01	97	01	01
HOMO−8	−7.13	0	100	0	0
HOMO−9	−7.13	0	100	0	0
HOMO−10	−7.42	02	77	15	06

Table 7
Energy and composition of selected molecular orbitals of complex **10**.

MO	Energy (eV)	% of composition			
		Mo	L	Oxo	brid
LUMO+5	−1.95	23	61	08	01
LUMO+4	−1.95	22	61	08	02
LUMO+3	−2.43	58	10	21	0
LUMO+2	−2.43	58	10	21	0
LUMO+1	−2.62	39	33	22	02
LUMO	−2.62	38	33	22	02
HOMO	−6.05	01	96($p\pi$ (S), 27)	01	02
HOMO−1	−6.05	01	96($p\pi$ (S), 27)	01	02
HOMO−2	−6.58	01	92($p\pi$ (S), 64)	05	02
HOMO−3	−6.58	01	91($p\pi$ (S), 63)	05	02
HOMO−4	−6.64	0	98($p\pi$ (S), 36)	0	02
HOMO−5	−6.64	0	98($p\pi$ (S), 37)	0	02
HOMO−6	−7.34	03	80	14	03
HOMO−7	−7.35	03	80	14	03
HOMO−8	−7.63	0	57	02	41
HOMO−9	−7.64	0	70	02	28
HOMO−10	−7.73	0	47	01	52

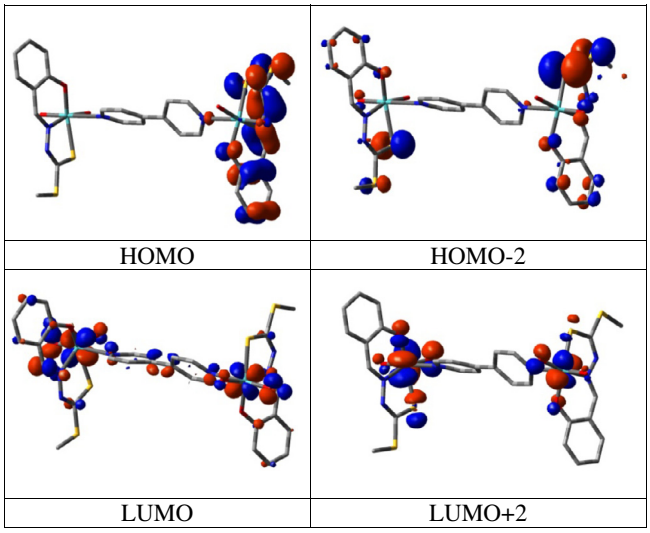

Fig. 8. Contour plots of selected molecular orbitals of complex **2**.

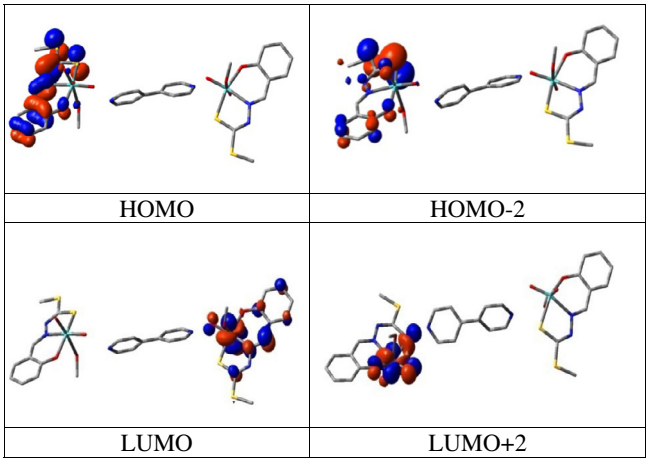

Fig. 9. Contour plots of selected molecular orbitals of complex **2a**.

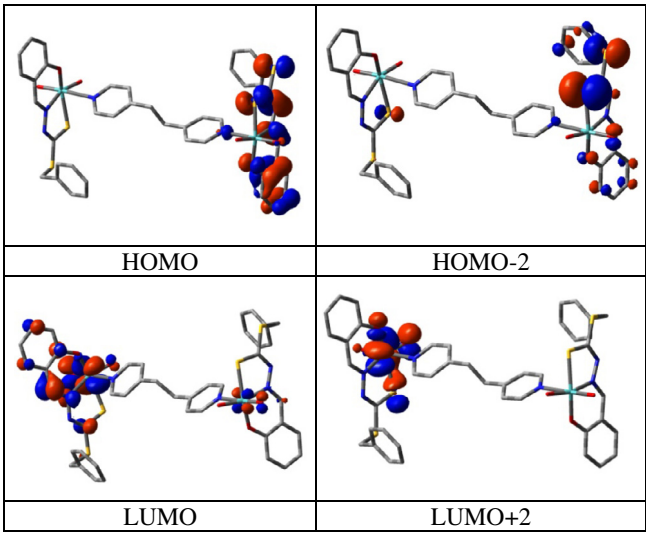

Fig. 10. Contour plots of selected molecular orbitals of complex **9**.

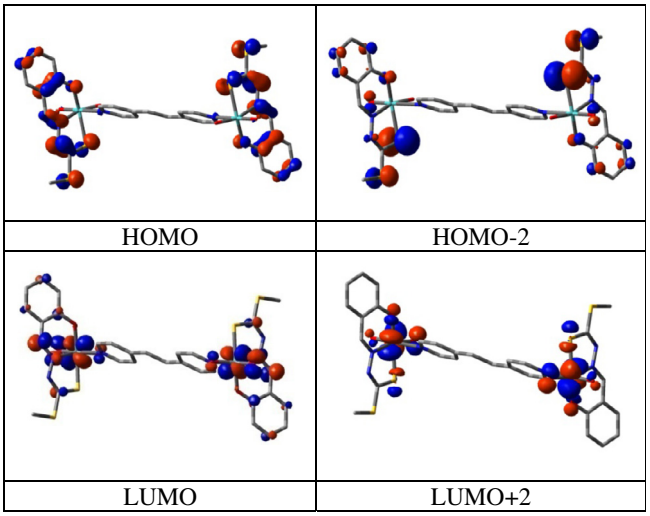

Fig. 11. Contour plots of selected molecular orbitals of complex **10**.

Table 8
Vertical electronic transitions calculated by TDDFT/CPCM method of complex **2**.

$E_{excitation}$ (eV)	$\lambda_{excitation}$ (nm)	Osc. Strength (f)	Key transitions	Character
2.3882	519.1	0.0117	(74%)HOMO → LUMO	π(L) → π^*(L)/$d\pi$(Mo)
2.3945	517.8	0.0113	(71%)HOMO−1 → LUMO	π(L) → π^*(L)/$d\pi$(Mo)
3.0869	401.7	0.0246	(39%)HOMO−4 → LUMO (26%)HOMO−5 → LUMO	π(L) → π^*(L)/$d\pi$(Mo)
3.0934	400.8	0.0240	(35%)HOMO−4 → LUMO+1 (22%)HOMO−5 → LUMO+1	π(L) → π^*(L)/$d\pi$(Mo)
3.4396	360.5	0.1311	(43%)HOMO−6 → LUMO (20%)HOMO−7 → LUMO+1	π(L) → π^*(L)/$d\pi$(Mo)
3.4796	356.3	0.2077	(42%)HOMO−7 → LUMO+1 (25%)HOMO−6 → LUMO	π(L) → π^*(L)/$d\pi$(Mo)
3.9540	313.6	0.1752	(62%)HOMO−3 → LUMO+6	$p\pi$(S) → π^*(L)
3.9556	313.4	0.1172	(64%)HOMO−2 → LUMO+6	$p\pi$(S) → π^*(L)

Table 9
Vertical electronic transitions calculated by TDDFT/CPCM method of complex **2a**.

$E_{excitation}$ (eV)	$\lambda_{excitation}$ (nm)	Osc. Strength (f)	Key transitions	Character
2.4393	508.3	0.0101	(80%)HOMO → LUMO	π(L) → π^*(L)/$d\pi$(Mo)
2.4728	501.4	0.0115	(82%)HOMO−1 → LUMO	π(L) → π^*(L)/$d\pi$(Mo)
3.0589	405.3	0.0317	(57%)HOMO−3 → LUMO (33%)HOMO−3 → LUMO+1	$p\pi$(S) → π^*(L)/$d\pi$(Mo)
3.2308	383.8	0.0461	(37%)HOMO → LUMO+5 (34%)HOMO−1→LUMO+5	π(L) → π^*(L)/$d\pi$(Mo)
3.5279	351.4	0.2063	(67%)HOMO−1 → LUMO+6	π(L) → π^*(L)/$d\pi$(Mo)
3.5346	350.8	0.2290	(65%)HOMO → LUMO+7	π(L) → $d\pi$(Mo)
4.0354	307.2	0.2368	(77%)HOMO−3 → LUMO+6	$p\pi$(S) → π^*(L)/$d\pi$(Mo)
4.0444	306.6	0.1602	(76%)HOMO−2 → LUMO+7	$p\pi$(S) → π^*(L)/$d\pi$(Mo)

Table 10
Vertical electronic transitions calculated by TDDFT/CPCM method of complex **9**.

$E_{excitation}$ (eV)	$\lambda_{excitation}$ (nm)	Osc. Strength (f)	Key transitions	Character
2.3347	531.1	0.0066	(75%)HOMO → LUMO	π(L) → π^*(L)/$d\pi$(Mo)
2.3405	529.7	0.0079	(78%)HOMO−1 → LUMO	π(L) → π^*(L)/$d\pi$(Mo)
3.0596	405.2	0.0335	(66%)HOMO−2 → LUMO+1	$p\pi$(S) → π^*(L)/$d\pi$(Mo)
3.0624	404.9	0.0560	(59%)HOMO−3 → LUMO	$p\pi$(S) → π^*(L)/$d\pi$(Mo)
3.1582	392.6	0.0332	(64%)HOMO−1 → LUMO+4	π(L) → π^*(L)/$d\pi$(Mo)
3.4390	360.5	0.0974	(56%)HOMO → LUMO+7	π(L) → π^*(L)/$d\pi$(Mo)
3.4433	360.1	0.1802	(55%)HOMO−1 → LUMO+6	π(L) → π^*(L)/$d\pi$(Mo)
4.0096	309.21	0.1327	(71%)HOMO−2 → LUMO+7	$p\pi$(S) → π^*(L)/$d\pi$(Mo)
4.0822	303.72	0.1425	(68%)HOMO−3 → LUMO+6	$p\pi$(S) → π^*(L)/$d\pi$(Mo)

Table 11
Vertical electronic transitions calculated by TDDFT/CPCM method of complex **10**.

$E_{excitation}$ (eV)	$\lambda_{excitation}$ (nm)	Osc. Strength (f)	Key transitions	Character
2.3881	519.2	0.0199	(48%)HOMO → LUMO (47%)HOMO−1 → LUMO	π(L) → π^*(L)/$d\pi$(Mo)
3.0940	400.7	0.0573	(35%) HOMO−5 → LUMO (28%)HOMO−4 → LUMO+1	π(L) → π^*(L)/$d\pi$(Mo)
3.2051	386.8	0.0407	(35%)HOMO−1 → LUMO+5 (34%)HOMO → LUMO+4	π(L) → π^*(L)/$d\pi$(Mo)
3.9568	313.3	0.1876	(39%)HOMO−3 → LUMO+6 (30%)HOMO−2 → LUMO+5	$p\pi$(S) → π^*(L)/$d\pi$(Mo)
3.9627	312.7	0.1427	(34%)HOMO−2 → LUMO+5 (29%)HOMO−3 → LUMO+6	$p\pi$(S) → π^*(L)/$d\pi$(Mo)

and their assignment are summarized in Tables 8–11. In the complexes very weak transitions at > 500 nm corresponding to HOMO/HOMO−1 → LUMO transitions (π(L) → π^*(L)/$d\pi$(Mo)) have been found which are not observed in the experimental spectra. However the moderately intense transitions corresponding to π(L) → π^*(L)/$d\pi$(Mo) and $p\pi$(S) → π^*(L)/$d\pi$(Mo) have been observed. The intense transitions at 300–360 nm having mixed π(L) → π^*(L)/$d\pi$(Mo) and $p\pi$(S) → π^*(L)/$d\pi$(Mo) character can be matched to the experimental bands.

4. Conclusions

The desired linear di-imine and di-amine bridged binuclear dioxomolybdenum(VI) complexes of the type [$(MoO_2L)_2$(B-B)] [where, B-B is a bidentate spacer 4,4′ bipyridine, 1,2 bis (4-pyridyl) ethene and 1,2 bis (4-pyridyl) ethane] have been synthesized and characterized by various physico-chemical techniques. Complexes **2**, **2a**, **9** and **10** were structurally characterized by single crystal X-ray crystallography. In each of the complexes, the centrosymmetric

structure consists of two MoO_2L moieties bridged by two N-atoms from di-imine/di-amine molecule which completes a distorted octahedral coordination environment around the Mo(VI) centers. The complexes also give rise to interesting supramolecular frameworks. DFT calculation on the ligand and the complexes **2**, **2a**, **9** and **10** were also carried out and the data were used to identify the composition of the relevant HOMOs and LUMOs and also to assign the experimentally observed transitions.

Acknowledgements

We are grateful to Dr. Ramaprasad Chakraborty, former Associate Professor, Bidhannagar College and Dr. Tapas Kumar Raychaudhuri for their constant support and interest in the work. We thank the University of Reading and the EPSRC (U.K) for funds for the Oxford Diffraction diffractometer.

Appendix A. Supplementary data

CCDC 979560–979563 contains the supplementary crystallographic data for **2**, **2a**, **9** and **10**. These data can be obtained free of charge via http://www.ccdc.cam.ac.uk/conts/retrieving.html, or from the Cambridge Crystallographic Data Centre, 12 Union Road, Cambridge CB2 1EZ, UK; fax: (+44) 1223-336-033; or e-mail: deposit@ccdc.cam.ac.uk. Supplementary data associated with this article can be found, in the online version, at http://dx.doi.org/10.1016/j.poly.2014.08.010.

References

[1] D. Collison, C.D. Garner, J.A. Joule, Chem. Soc. Rev. 25 (1996) 25.
[2] R. Hill, Chem. Rev. 96 (1996) 2757.
[3] R.K. Grasselli, Catal. Today 49 (1999) 141.
[4] R.J. Cross, P.D. Newman, R.D. Peacock, D. Stirling, J. Mol. Catal. 144 (1999) 273.
[5] K.J. Ivin, J.C. Mol, Olefin Metathesis Polymerization, Academic Press, London, 1997.
[6] R.H. Holm, Chem. Rev. (1987) 1401.
[7] (a) M.D. Ward, Chem. Soc. Rev. 24 (1995) 121;
(b) M.D. Ward, Chem. Ind. 15 (1996) 568.
[8] (a) S.R. Batten, R. Robson, Angew. Chem., Int. Ed. 37 (1998) 1460;
(b) S. Kitagawa, M. Kondo, Bull. Chem. Soc. Jpn. 71 (1998) 1735;
(c) A.J. Blake, N.R. Champness, P. Hubberstey, W.S. Li, M.A. Withersby, M. Schröder, Coord. Chem. Rev. 183 (1999) 117.
[9] J.A. MaCleverty, M.D. Ward, Acc. Chem. Res. 31 (1998) 842.
[10] (a) P.J. Zapf, R.C. Haushalter, J. Zubieta, Chem. Commun. (1997) 321;
(b) P.J. Zapf, R.C. Haushalter, J. Zubieta, Chem. Mater. 9 (1997) 2019;
(c) P.J. Zapf, R.L. LaDuca, R.S. Rarig, K.M. Johnson III, J. Zubieta, Inorg. Chem. 37 (1998) 3411;
(d) P.J. Zapf, C.J. Warren, R.C. Haushalter, J. Zubieta, Chem. Comm. (1997) 1543;
(e) D. Hagram, C. Zubieta, D.J. Rose, R.C. Haushalter, J. Zubieta, Angew. Chem., Int. Ed. 36 (1997) 795.
[11] B.K. Koo, H. Kang, W.T. Lim, Bull. Korean Chem. Soc. 29 (2008) 1819.
[12] H. Kang, W.T. Lim, B.K. Koo, J. Korean Chem. Soc. 52 (2008) 439.
[13] (a) S.I. Stupp, L.C. Palmer, Chem. Mater. 26 (2014) 507;
(b) F. Faridbod, M.R. Ganjali, R. Dinarvand, P. Norouzi, S. Riahi, Sensors 8 (2008) 1645.
[14] N.R. Pramanik, S. Ghosh, T.K. Raychaudhuri, S. Ray, Ray J Butcher, S.S. Mandal, Polyhedron 23 (2004) 1595.
[15] N.R. Pramanik, S. Ghosh, T.K. Raychaudhuri, S. Chaudhuri, M.G.B. Drew, S.S. Mandal, J. Coord. Chem. 60 (2007) 2177.
[16] A.D. Becke, J. Chem. Phys. 98 (1993) 5648.
[17] C. Lee, W. Yang, R.G. Parr, Phys. Rev. B. 37 (1988) 785.
[18] P.J. Hay, W.R. Wadt, J. Chem. Phys. 82 (1985) 270.
[19] W.R. Wadt, P.J. Hay, J. Chem. Phys. 82 (1985) 284.
[20] P.J. Hay, W.R. Wadt, J. Chem. Phys. 82 (1985) 299.
[21] R. Bauernschmitt, R. Ahlrichs, Chem. Phys. Lett. 256 (1996) 454.
[22] R.E. Stratmann, G.E. Scuseria, M.J. Frisch, J. Chem. Phys. 109 (1998) 8218.
[23] M.E. Casida, C. Jamorski, K.C. Casida, D.R. Salahub, J. Chem. Phys. 108 (1998) 4439.
[24] V. Barone, M. Cossi, J. Phys. Chem. A 102 (1998) 1995.
[25] M. Cossi, V. Barone, J. Chem. Phys. 115 (2001) 4708.
[26] M. Cossi, N. Rega, G. Scalmani, V. Barone, J. Comput. Chem. 24 (2003) 669.
[27] Gaussian 09, Revision D.01, M.J. Frisch, G.W. Trucks, H.B. Schlegel, G.E. Scuseria, M.A. Robb, J.R. Cheeseman, G. Scalmani, V. Barone, B.Mennucci, G.A. Petersson, H. Nakatsuji, M. Caricato, X. Li, H.P. Hratchian, A.F. Izmaylov, J. Bloino, G. Zheng, J.L. Sonnenberg, M. Hada, M. Ehara, K. Toyota, R. Fukuda, J. Hasegawa, M. Ishida, T. Nakajima, Y. Honda, O. Kitao, H. Nakai, T. Vreven, J.A. Montgomery, Jr., J.E. Peralta, F. Ogliaro, M. Bearpark, J.J. Heyd, E. Brothers, K.N. Kudin, V.N. Staroverov, R. Kobayashi, J. Normand, K. Raghavachari, A. Rendell, J.C. Burant, S.S. Iyengar, J. Tomasi, M. Cossi, N. Rega, J.M. Millam, M. Klene, J.E. Knox, J.B. Cross, V. Bakken, C. Adamo, J. Jaramillo, R. Gomperts, R.E. Stratmann, O. Yazyev, A.J. Austin, R. Cammi, C. Pomelli, J.W. Ochterski, R.L. Martin, K. Morokuma, V.G. Zakrzewski, G.A. Voth, P. Salvador, J.J. Dannenberg, S. Dapprich, A.D. Daniels, Ö. Farkas, J.B. Foresman, J.V. Ortiz, J. Cioslowski, D.J. Fox, Gaussian Inc, Wallingford CT, 2009.
[28] N.M. O'Boyle, A.L. Tenderholt, K.M. Langner, J. Comput. Chem. 29 (2008) 839.
[29] E.I. Stiefel, Prog. Inorg. Chem. 22 (1977) 1.
[30] R. Dinda, P. Sengupta, T.C.W. Mak, S. Ghosh, Inorg. Chem. 41 (2002) 1684.
[31] A. Rana, R. Dinda, P. Sengupta, S. Ghosh, Larry R. Falvello, Polyhedron 21 (2002) 1023.
[32] S.K. Dutta, D.B. McConville, W.J. Youngs, M. Chaudhury, Inorg. Chem. 36 (1997) 2517.
[33] Y.-L. Zhai, X.-X. Xu, X. Wang, Polyhedron 11 (1992) 415.
[34] M. Chaudhury, J. Chem. Soc., Dalton Trans. (1984) 115.
[35] R.H. Holm, P. Kennepohl, E.I. Solomon, Chem. Rev. (1996) 2239.
[36] S. Bhattacharyya, S.B. Kumar, S.K. Dutta, E.R.T. Tiekink, M. Chaudhury, Inorg. Chem. 35 (1996) 1967.
[37] M. Chaudhury, Inorg. Chem. 24 (1985) 3011.
[38] S. Purohit, A.P. Koley, L.S. Prasad, P.T. Manoharan, S. Ghosh, Inorg. Chem. 28 (1989) 3735.
[39] A.P. Koley, S. Purohit, S. Ghosh, L.S. Prasad, P.T. Manoharan, J. Chem. Soc., Dalton Trans. (1988) 2607.
[40] C. Bustos, O. Burckhardt, R. Schrebler, D. Carrillo, A.M. Arif, A.H. Cowley, C.M. Nunn, Inorg. Chem. 29 (1990) 3996.
[41] J.A. Craig, E.W. Harlan, B.S. Snyder, M.A. Whitener, R.H. Holm, Inorg. Chem. 28 (1989) 2082.
[42] R. Hahn, U. Kusthardt, W. Scherer, Inorg. Chim. Acta 210 (1993) 177.
[43] M.W. Bishop, J. Chatt, J.R. Dilworth, M.B. Hursthouse, S. Amarasiri, A. Jayaweera, A. Quick, J. Chem. Soc., Dalton Trans. (1979) 941.
[44] M.W. Bishop, J. Chatt, J.R. Dilworth, M.B. Hursthouse, M. Motevalli, J. Chem. Soc., Dalton Trans. (1979) 1603.
[45] S. Alghool, C. Slebodnick, Polyhedron 67 (2014) 11.
[46] S. Marivel, M. Arunachalam, P. Ghosh, Cryst. Growth Des. 11 (2011) 1642.
[47] L.M. Gregoret, S.D. Rader, R.J. Fletterick, F.E. Cohen, Proteins Struct. Funct. Genetics 9 (1991) 99.
[48] U.P. Singh, S. Kashyap, H.J. Singh, Ray J. Butcher, Cryst. Eng. Commum. 13 (2011) 4110.